

Spin-Dependent Lifetime and Exchange Splitting of Surface States on Ni(111)

Beatrice Andres, Paul Weiss, Marko Wietstruk, Martin Weinelt

Freie Universität Berlin, Fachbereich Physik, Arnimallee 14, 14195 Berlin, Germany

E-mail: weinelt@physik.fu-berlin.de

Abstract. We report on a spin-resolved two-photon photoemission study of the Ni(111) surface states. Nickel thin films were grown by molecular beam epitaxy on a W(110) substrate. The first image-potential state is used as a sensor to map the spin polarization of the occupied surface states. This allows us to identify the majority spin component of the Shockley surface state as well as a majority and minority d -derived surface resonance. The $n = 1$ image-potential state is found to be exchange split by 14 ± 3 meV. In spite of the fact that the band structure at the Fermi level exhibits a strongly discerned density of states in both spin channels, we observe low spin asymmetries in the decay and dephasing rates of the photoexcited electrons. Varying the sample preparation reveals that the Shockley surface state contributes about 40 % to the spin-dependent decay rate.

Submitted to: *J. Phys.: Condens. Matter*

PACS numbers: 78.47.-p; 73.20.At; 75.70.Ak

1. Introduction

The exchange splitting of the Ni 3d states results in a variety of phenomena interesting for both applications and fundamental science. One example of current interest is the highly spin-polarized tunneling current emitted from a nickel tip [1], which promises Ni as an efficient material for spin injection. Another observation is a high spin polarization in secondary electron emission from graphene/Ni(111) even under oxygen exposure [2], which allows for a potential application of the graphene/Ni(111) system in spintronic devices. In Ref. [2] the microscopic origin of this high spin polarization in secondary electron emission is proposed to be spin-flip scattering between the hot electrons and the 3d valence electrons of Ni. Although, spin-flip contributions and magnon emission are of low significance to the decay of hot electrons in Ni according to first-principle calculations of Zhukov *et al.* [3].

Spin-resolved two-photon-photoemission (2PPE) provides the means to unravel spin-flip and non-spin-flip contributions to electronic scattering. We investigate the spin-dependent decay and dephasing rates of electrons excited into the image-potential states of the Ni(111) surface. The image-potential states are well-defined surface states energetically bound to the vacuum level [4].

The main decay mechanism for excited electrons is inelastic electron-electron scattering whereby the primary electron transfers its energy to a secondary electron-hole pair [5]. Therefore this process is dominated by the occupied and unoccupied electronic states around the Fermi level which closely connects the spin-dependent density of states (DOS) to the lifetime of excited majority and minority spin electrons. To gain a thorough understanding of these scattering processes a detailed knowledge of the spin-split electronic structure around the Fermi level is crucial.

During the last three decades the band structure of the Ni(111) surface has been calculated [6, 7, 8, 9, 10] and investigated by means of photoemission [11, 12, 13, 14, 15], inverse photoemission [16] and scanning tunneling spectroscopy [6, 13, 17]. The close-packed surface exhibits the well-known Shockley surface state. Its spin splitting and position with respect to the Fermi energy E_F are still subject of controversy. At the center of the Brillouin zone Γ the Shockley surface state was found to be either occupied in both spin components [17] or occupied in the majority component and unoccupied in the minority channel [10, 13, 18] or even unoccupied in both spin parts [6]. A second surface resonance of *d*-character was predicted in surface-band-structure calculations [10] and was observed in the majority of photoemission experiments [11, 19]. Recently even a third surface resonance was found by Lobo-Checa *et al.* [7] with an exchange splitting quantified one year later by Okuda *et al.* [20]. In addition, for 1 to 21 monolayer (ML) thick Ni(111) films on W(110) angle-resolved photoemission spectroscopy shows quantum-well states (QWS) close below the Fermi level [21]. Nevertheless, in our measurements we neither observe QWS signatures in photon-energy-dependent measurements nor a QWS influence to the lifetimes of laser-excited electrons.

In the present study we take advantage of 2PPE to project the occupied part of

the surface DOS close below E_F onto the intermediate image-potential states [22]. As described in Section 3 the two-step photoexcitation process allows us to identify the Ni surface states according to their spin character and symmetry. Section 4 discusses the binding energy, exchange splitting and spin-dependent scattering rates of the first and second image-potential states. The experiment is briefly described in the following section.

2. Experiment

When 2PPE is applied to a ferromagnet, a first laser pump pulse excites electrons from an occupied initial state into an unoccupied intermediate state thereby maintaining the spin polarization of the initial state. For the Ni(111) surface we map the spin polarization of the occupied surface states serving as initial states onto the unoccupied image-potential states serving as intermediate states (illustrated in Fig. 1). Using a time-delayed laser probe pulse we can directly access the spin-dependent relaxation times of the excited electrons [23].

For the 2PPE spectra shown in this paper pump and probe pulses are generated by a home-built Ti:Sapphire oscillator. After excitation by the probe photon the electron trapped in the image potential can overcome the work function Φ of the Ni(111) surface and is photoemitted. For probe we use the laser fundamental ($h\nu$) which is tunable from 1.49 to 1.67 eV. The pump pulses are created by frequency tripling the fundamental to $3h\nu = 4.47 - 5.01$ eV. The kinetic energy and spin polarization of the photoemitted electrons are detected in normal emission by a cylindric sector analyzer (CSA 300, Focus) combined with spin-polarized low-energy electron diffraction (SP-LEED). Energy and angular resolution are 65 meV and $\pm 5^\circ$, respectively. A detailed description of the experimental setup has been published previously in Ref. [24].

2.1. Sample preparation

For the investigations in this paper thin nickel films from 7 to 14 monolayers (ML) were deposited onto a W(110) substrate using a commercial EFM3 UHV evaporator (Focus / Omicron) at an operating pressure of 2×10^{-10} mbar. Beforehand, the W(110) substrate was cleaned from carbon impurities by heating in oxygen atmosphere at a partial pressure of 2×10^{-7} mbar and a temperature of 1800 K for 60 hours with repetitive flashes to 2200 K every 8 hours in order to desorb tungsten oxide [25]. We started evaporating Ni at a substrate temperature of 573 K, while the tungsten crystal was cooling down from a 2200 K flash. For the remaining evaporation process the substrate was kept at a temperature of 443 K. To obtain a smooth and contaminant-free surface, the Ni films were annealed for 3 minutes at 573 K after moving to the measurement position. The surface structure of the W(110) substrate and the evaporated Ni(111) film was controlled by LEED. The Ni film-thickness was determined subsequently to the 2PPE measurements by thermal desorption spectroscopy (TDS). All temperatures

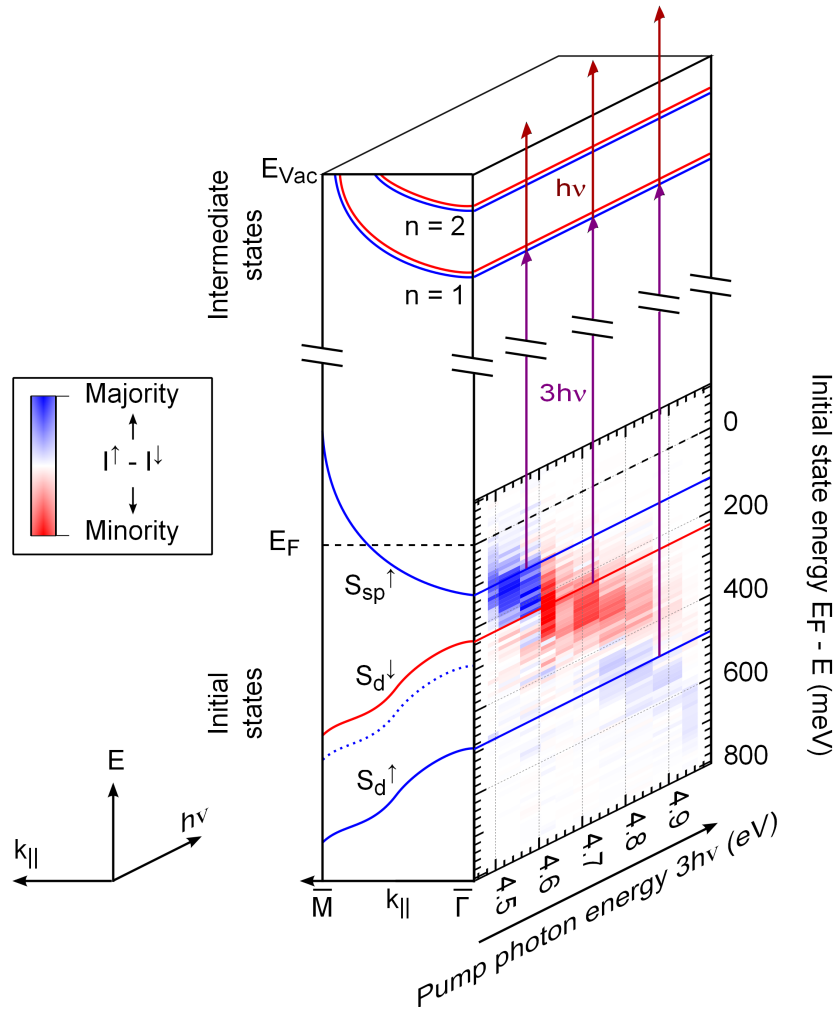


Figure 1. Sketch of the 2PPE excitation process for three different pump/probe photon energies. On the $k_{||}$ - E plane (front plane) all states involved in the 2PPE process are displayed in a schematic drawing of the surface band structure. By photon energy variation the $n = 1$ image-potential state is pumped from different initial states (S_{sp}^{\uparrow} , S_d^{\downarrow} , S_d^{\uparrow}) leading to a varying spin polarization observed in the image-potential state. The intensity difference $I^{\uparrow} - I^{\downarrow}$ between the majority and minority spin spectra (from Fig. 2) is shown on the E - $h\nu$ plane (right-hand side) on the energy scale of the initial states. Positive (majority) values are colored in blue, negative (minority) values in red.

were measured with a thermocouple (type C) directly attached to the tungsten crystal.

Since we deposit our Ni thin films at higher temperatures than in Ref. [21] to improve the surface quality, it is reasonable that the W/Ni interface is roughened which suppresses the formation of QWS. That is why in the following we conclude that all our observed features are characteristic for the surface of a Ni(111) bulk crystal.

2.2. Two-photon photoemission spectroscopy

For the 2PPE measurements we cooled the sample to a temperature of 90 K with liquid nitrogen. The pressure during data recording was 2×10^{-11} mbar. All spectra were taken for normal electron emission, *i.e.*, at the center of the surface Brillouin zone $\bar{\Gamma}$. Both laser pulses were *p*-polarized and incident at an angle of 80° off normal along the $W[1\bar{1}0]$ direction, corresponding to the $Ni[\bar{1}\bar{1}2]$ direction. The advantage of this grazing incidence geometry is that transitions from states of Λ_1 symmetry into the free-electron-like image-potential state [27] have the highest probability. While a very small component of the laser field is applicable for transitions from Λ_3 states. Thus we detect the spin polarization of the Λ_1 -symmetric surface states close below E_F with hardly any background from the overlapping Λ_3 bulk bands.

The Ni films were magnetized remanently in plane along the $Ni[1\bar{1}0]$ direction applying a field pulse of 20 mT via a freestanding coil.

The work function of the analyzer is 4.22 ± 0.01 eV. No bias was applied to the samples during the measurements.

3. Surface states near the Fermi level

By tuning the photon energy $3h\nu$ of the pump pulse we select different initial states from below the Fermi level E_F to populate the unoccupied $n = 1$ image-potential state. Figure 1 illustrates the excitation scheme for three different photon energies $3h\nu$ suitable for excitations from the three states $S_{sp}^\uparrow, S_d^\downarrow$ and S_d^\uparrow . Since the spin is conserved in the optical dipole transitions, the spin character of the initial state determines the spin polarization of the 2PPE final state.

Figure 2 displays a series of 2PPE spectra taken at increasing pump photon energies (on a type B sample, see Sec. 4.1). Minority and majority spin channels are shown in the left and right panels, respectively. Referencing the 2PPE data to E_F , the initial state energy is fixed in this representation while the intermediate image-potential state shifts with the pump photon-energy variation $\Delta 3h\nu$. As initial states we find the three distinct surface state components, that are shown in the front plane of Fig. 1. One can be identified as the occupied part of the Shockley surface state S_{sp} (in Refs. [7, 9, 20] referred to as S_1) which is discussed in Sec. 3.2. The other two belong to *d*-derived surface resonances S_d (S_2 in Refs. [7, 9, 20]) as discussed in the following.

3.1. *d*-derived surface resonances

Surface-state electrons compared to electrons in bulk states are more likely to be laser-excited into the image potential since both, surface and image-potential states have a high probability density at the surface and thus large spatial overlap. This shows up in a significantly higher 2PPE intensity if the photon energy is resonant to the energy difference between an occupied surface and the image-potential state. Such a resonance is visible in the minority-spin spectra in Fig. 2 at 4.62 eV pump photon energy (left

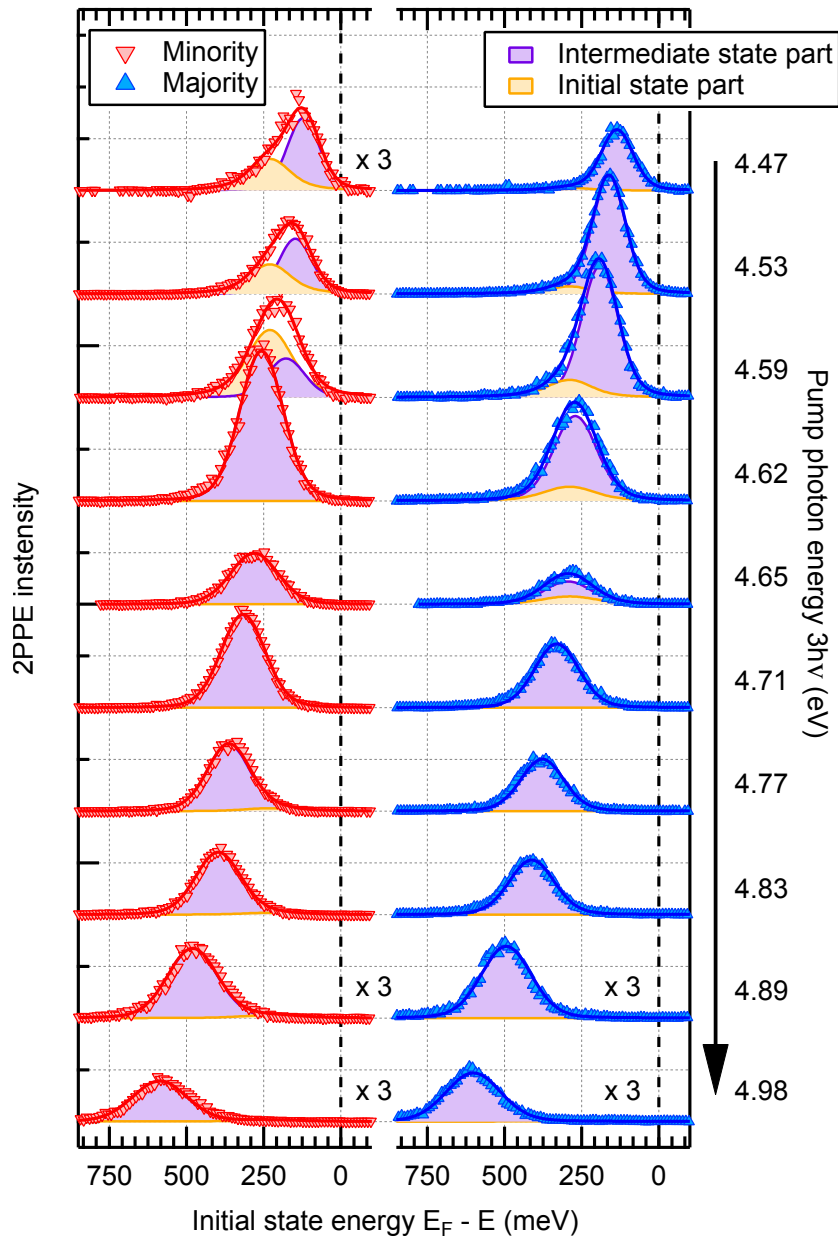


Figure 2. 2PPE spectra for minority and majority spins (left and right panels) of a 7ML Ni/W(110) film (on a type B sample, see Sec. 4.1). The photon energy of the $3h\nu$ pump pulse increases from 4.47 to 4.98 eV. Spectra are recorded in normal emission for zero time delay between pump and probe pulses at a sample temperature of 90 K. The spectra have been fitted (solid lines) using a combination of two Voigt profiles accounting for the initial (solid, light yellow) and intermediate (solid, purple) state contribution to the 2PPE signal.

panel). In addition at lower photon energies the peaks show a clearly asymmetric line shape. This is the manifestation of an initial surface state with significant spectral weight contributing to the 2PPE intensity besides the intermediate image-potential-state peak. Accounting for this we fitted the spectra using the superposition of two Voigt profiles representing the initial and intermediate state contributions to the 2PPE signal. We obtained the best fit results when fixing the initial-state binding energy at 230 meV, the energetic position of a spin-split d -derived minority surface state S_d^\downarrow [20]. This state has also been found at 230 meV in spin-integrated 1PPE and 2PPE [11] measurements. The asymmetry vanishes when going to photon energies higher than the resonance and only the intermediate-state peak remains. Such a behavior is not unusual in 2PPE. It has also been observed on Si(001) and explained by a Fano resonance due to the interference of bulk and surface transitions [26].

In Ref. [20] a surface contribution in the majority spin channel of spin-resolved photoemission was found at 289 ± 4 meV and identified as the majority counterpart S_d^\uparrow of this d -derived surface state. At this energy we fixed a majority feature in our fits to account for the asymmetric line shape of the majority spin spectra at low photon energies (see Fig. 2 right panel). An explanation for the lower intensity of S_d^\uparrow as compared to S_d^\downarrow is given by DFT [7] and Green's function calculations [9], which predict that the majority component of this d -derived surface state does not contribute to the electronic spectral weight. In contradiction to this assignment the exchange splitting of the d -derived surface resonance is significantly larger according to Refs. [7, 9]. They assign a binding energy of around 500 meV to the majority component. Figure 1 shows the intensity difference $I^\uparrow - I^\downarrow$ between minority and majority spin channels extracted from the spectra in Fig. 2. This reveals a majority-spin intensity rising from 500 meV towards higher binding energies. We can rule out that this feature stems from the exchange split bulk band of Λ_3 symmetry existing in this energy region because of two reasons. First, as mentioned above in Sec. 2.2, using p -polarized light at an incidence angle of 80° , we have a very low transition probability from Λ_3 bulk bands into the Λ_1 -symmetric image-potential state. Second, we do not observe a reversal of the spin polarization between 526 ± 2 meV where the minority part is situated [20] and 694 ± 6 meV which is the binding energy of the majority part. Thus we find two majority-spin surface resonances of which one likely constitutes the majority-spin S_d^\uparrow partner of the exchange-split d -like surface resonance: A weak majority-spin surface resonance at 289 meV and a second, broad majority-spin surface resonance at around 500 meV (indicated by dashed and solid blue lines in Fig. 1, front plane). From our observations we can not distinguish which of these two features is the S_d^\uparrow .

3.2. Shockley surface state

Lowering the photon energy from $3h\nu = 4.98$ eV to 4.47 eV, *i.e.*, probing initial states closer to E_F , the spin polarization changes from majority to minority and back to majority (see Fig. 1). The first reversal at a photon energy of 4.80 eV is caused by a

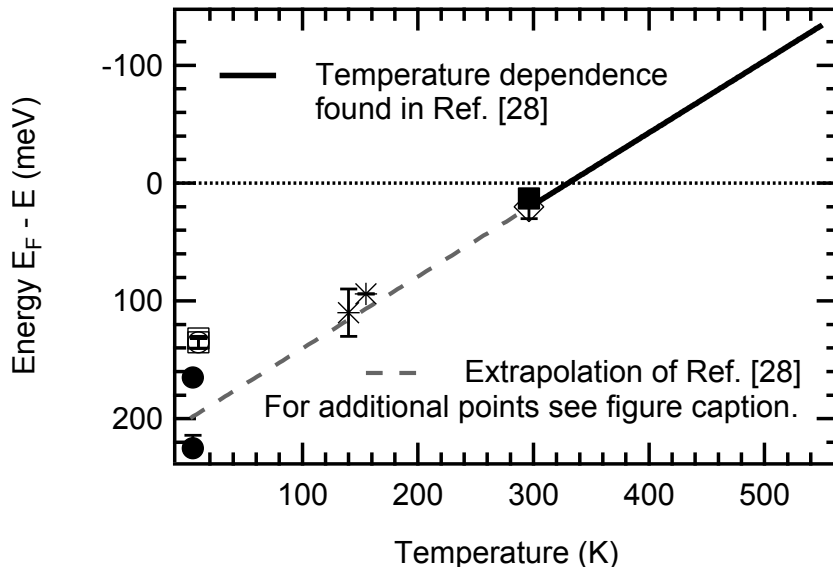


Figure 3. Temperature dependence of the majority component of the Shockley surface state. The solid black line shows the behavior found in Ref. [28], the dashed grey line is an extrapolation to lower temperatures that matches the previously known values. Single data points are taken from Refs. [20] (■), [7] (◇), [11] (*), [12] (○), [13] (□) and [17] (●).

resonance between the dominant minority surface d -resonance and the image-potential state. We assign the second transition at 4.60 eV to a nearing resonance with the majority part of the spin-split Shockley surface state S_{sp}^{\uparrow} . The strong majority character close to E_F (see also the spin polarization of the $n = 2$ image-potential state in Fig. 5) confirms that the minority component is situated at higher energies above E_F and is thus completely unoccupied corroborating the results of Refs. [10, 13, 18].

From the rising majority spin polarization in our low-photon-energy spectra we can estimate an energy position $E_F - E \leq 150$ meV. This value is in between the known results ranging from 94 meV [11] to 225 meV [17] below E_F . To unify the various results, we need to remember that the binding energy of the Shockley surface state on Ni(111) is, as on the noble metal surfaces, strongly temperature-dependent. A shift of 0.61 ± 0.1 meV/K has been observed [28] for increasing temperature from 300 K to the Curie temperature of $T_C = 631$ K. As compiled in Fig. 3 the diversity of known binding energies can be brought onto a line according to this temperature dependence even for temperatures below 300 K [7, 11, 12, 13, 17, 20]. Measured at a temperature of ≈ 90 K the binding energy we find is in accordance with the temperature dependent shift.

4. Surface states at the vacuum level

The Rydberg-like series of unoccupied image-potential states close below the vacuum energy has been resolved on Ni(111) first by Fischer *et al.* [5] in a 2PPE experiment. An exchange splitting of 18.2 ± 2.5 meV was deduced for the first image-potential state

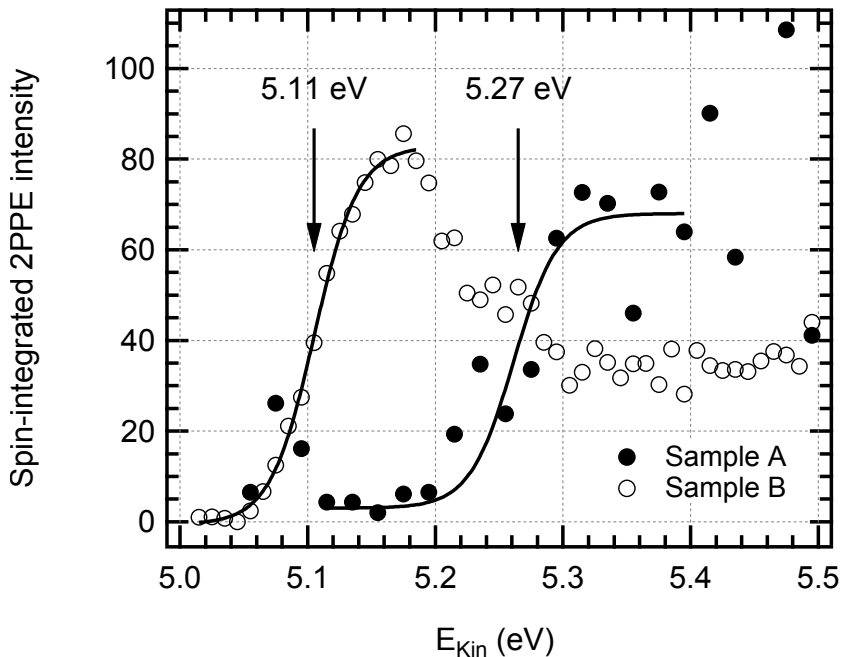


Figure 4. The secondary cutoff for type A and type B samples is observed at different kinetic energies. This difference shows a reduction in the samples work function from $\Phi_A = 5.27 \pm 0.03$ eV to $\Phi_B = 5.11 \pm 0.03$ eV depending on the temperature ramp rate during annealing which is 2 K/s for type A and > 2 K/s for type B. The spectrum shown here representative for type A samples has been collected at $3h\nu = 5.01$ eV, the type B spectrum at $3h\nu = 4.96$ eV. Both samples had a thickness of 7 ML as controlled by TDS.

(quantum number $n = 1$) by spin-resolved inverse photoemission (IPE) [29]. As the binding energy of image-potential states refers to the vacuum level E_{vac} , it is necessary to know the sample work-function to establish their binding energies.

4.1. Work function of Ni(111) thin films on W(110)

The work function is derived from the low-energy cutoff in the 2PPE spectrum at normal emission. A distinct low-energy cutoff in the Ni(111) 2PPE spectra can be observed at high photon energies (see Fig. 4) stemming from thermally and optically excited electrons above E_F . We deduce two different work functions from this cutoff for Ni films of equal thickness depending on the temperature ramp during annealing: For a ramp rate of 2 K/s (referenced in the following as sample type A) we obtain $\Phi_A = 5.27 \pm 0.03$ eV while for higher ramp rates (sample type B) we find $\Phi_B = 5.11 \pm 0.03$ eV. Both values are close to the work function of ≈ 5.22 eV reported for Ni(111) single crystal surfaces [5, 11, 19, 30].

An explanation for the two different work functions is the well-known Smolouchowski effect [31]. We expect the Ni films annealed at a faster temperature ramp to show higher surface roughness, *i.e.*, an increased step density than those

Table 1. Binding energy $E - E_{\text{vac}}$ and exchange splitting of the $n = 1$ and 2 image-potential states on the Ni(111) surface. For the values measured by spin-resolved IPE (srIPE) we assume the most frequently observed work function of 5.25 eV. All previously derived energies were determined for Ni(111) single crystals.

n	E_{\uparrow} (meV)	E_{\downarrow} (meV)	$\Delta E_{\uparrow/\downarrow}$ (meV)	Reference
1	736 ± 2	722 ± 2	14 ± 3	This work
	686.0 ± 1.8	667.8 ± 1.8	18.2 ± 2.5	srIPE [29]
	770 ± 30			2PPE [30]
2	183 ± 15	171 ± 17	12 ± 12	This work
	250 ± 50			2PPE [34]
	270 ± 30			2PPE [35]

annealed slower. This increased step density can lead to the lowered work function Φ_{B} . Additionally, electrons emitted from lower terraces between higher islands can lead to the observation of a lower cutoff at a nominal thickness of 7 ML, since thinner Ni/W(110) films exhibit smaller work functions [32, 33].

4.2. Binding energies of the image-potential states

The binding energies of the image-potential states relative to E_{vac} do not change from type A to type B samples. Fig. 5 shows a spin-resolved 2PPE spectrum recorded on a type A sample at $h\nu = 1.67$ eV and $3h\nu = 5.01$ eV. The high photon energy allows to excite both, the exchange-split $n = 1$ and $n = 2$ image-potential states close to E_{vac} . The low intensity of the $n = 2$ compared to the $n = 1$ image-potential state indicates that the former is populated from initial states with very low electron occupation, *i.e.*, thermally excited electrons close above E_{F} . However, the positive spin polarization of the $n = 2$ image-potential state confirms the majority spin character of the initial Shockley state around E_{F} .

Binding energies and exchange splittings of the image-potential states are summarized in Table 1. From the fits in Figs. 2 and 5 we extract an exchange splitting of $\Delta E_1^{\uparrow\downarrow} = 14 \pm 3$ meV for the $n = 1$ image-potential state, which is very close to what we would expect from the following consideration: The energy of the image-potential states depends on the position of the *sp*-derived band-gap edges [36]. Thus the exchange-split valence bands induce the exchange splitting of the image-potential states, which therefore is expected to scale with their bulk penetration. We calculated a bulk penetration of 5.7% in a 1D-model of the image potential using the Ni band gap edges [10] for solving a two-band model of the bulk band-structure as described in Ref. [36]. Given that at the Ni(111) surface only 5.7% of the probability density of the $n = 1$ image-potential state reside within the crystal and that the valence bands of Ni are exchange split by about 300 meV [37] we estimate the $n = 1$ exchange splitting to

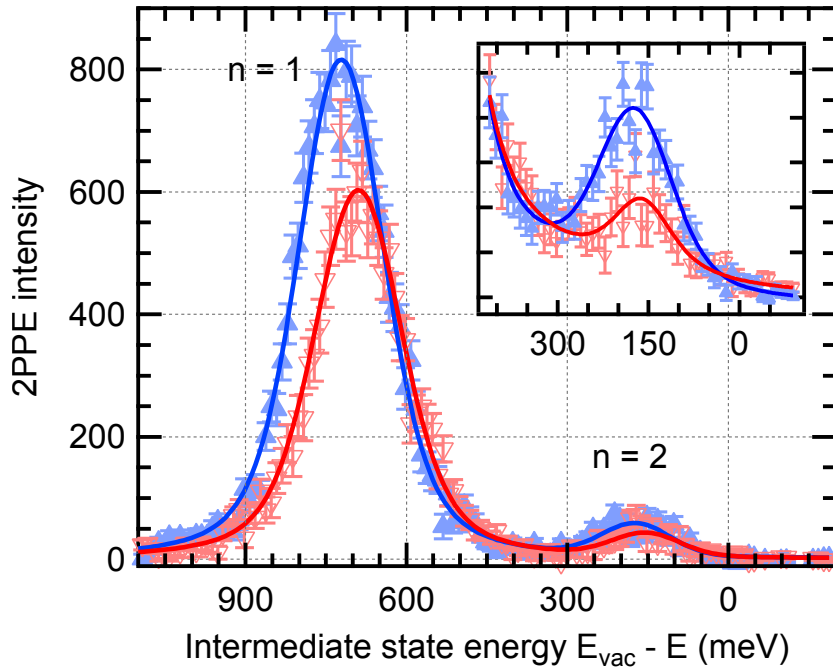


Figure 5. 2PPE spectrum of the $n = 1$ and $n = 2$ image-potential states at zero pump-probe delay. The high photon energy ($3h\nu = 5.01$ eV) allows to populate the $n = 2$ image-potential state with electrons excited close above E_F . This leads to the significantly lower intensity compared to the $n = 1$ image-potential state populated from S_a^\uparrow .

16 meV. This agrees well with the experimentally determined value.

Due to our low intensities in the $n = 2$ image-potential state we can only roughly estimate the exchange splitting to $\Delta E_2^{\uparrow\downarrow} = 12 \pm 12$ meV. Since $\Delta E_2^{\uparrow\downarrow}$ also scales with the bulk penetration ($\propto n^3$) it is expected to be smaller than $\Delta E_1^{\uparrow\downarrow}$ by a factor of 8. This scaling has been observed for 3 ML Fe on Cu(100) [24].

4.3. Lifetimes

Performing time-resolved 2PPE measurements with the electron analyzer tuned to the kinetic energy of the majority and minority $n = 1$ image-potential state, we can deduce the spin-dependent lifetimes of electrons excited to this state. The top part of Fig. 6 shows such spin- and time-resolved 2PPE traces of the $n = 1$ image-potential states on a type A and a type B sample. For comparison, the cross correlation determined in parallel by 2PPE measurements of the occupied Shockley surface state on Cu(111) [39] is also shown. The temporal evolution of the $n = 1$ image-potential-state population on Ni(111) is identical to the shape of the cross correlation. This indicates that the lifetimes are small compared to the 110 fs full width at half maximum of the cross correlation. Nevertheless we observe a shift between the cross correlation measured on Cu(111) and the majority and minority image-potential-state signals of Ni(111) which is indicated in Fig. 6 by the blue and red vertical lines offset with respect to the dashed line at zero

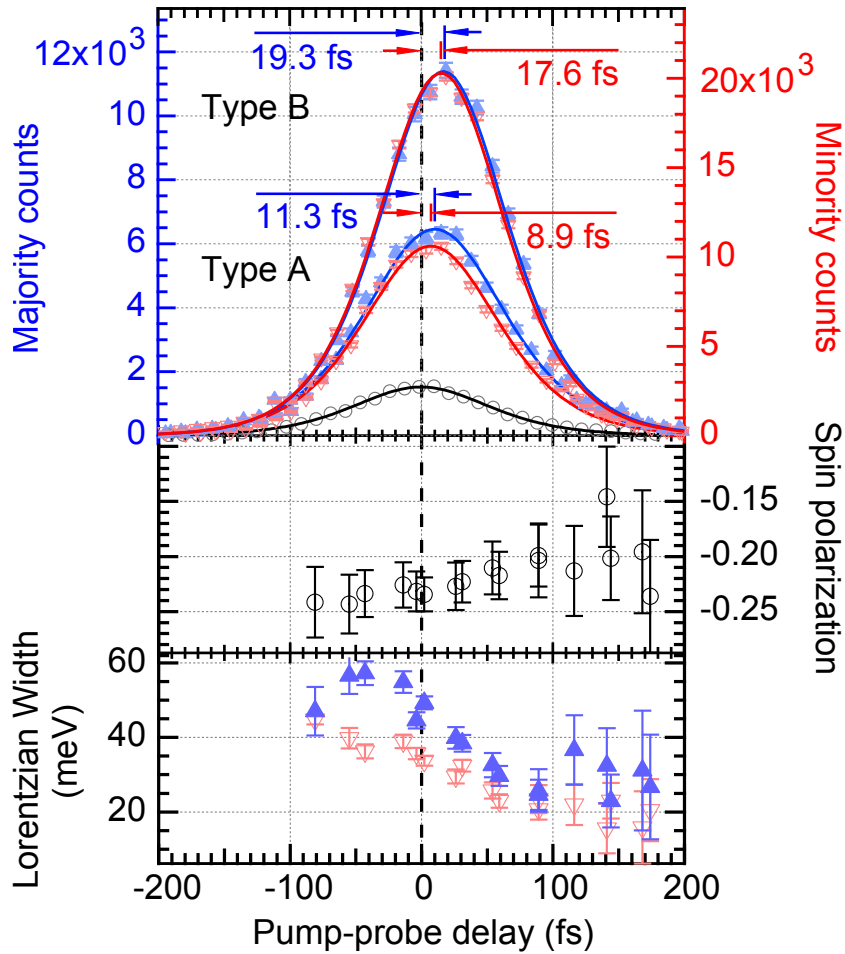


Figure 6. Top: Time- and spin-resolved measurement taken with the electron analyzer-energy tuned to the peak maximum of the majority and minority spin component of the $n = 1$ image-potential state. The two time-resolved traces stem from samples A and B and show distinct shifts with respect to delay zero. Up (blue) and down (red) triangles show the majority and minority spin contribution to the 2PPE intensity. The cross correlation is shown in black according to the majority intensity scale. The middle and bottom panels show the temporal evolution of the spin polarization and of the linewidth of the $n = 1$ image-potential states of the type A sample, respectively. All spectra were taken at a pump-photon energy of $3h\nu = 4.71$ eV.

pump-probe delay. It has been shown that this shift resembles the lifetime for systems with fast electronic decay measured with comparatively long laser pulses [38].

Unlike the image-potential-state binding energies, their lifetimes do show a dependence on the annealing procedure. The lifetimes and spin asymmetries we determined for the two sample types are summarized in Table 2. The lifetimes found on the higher-work-function samples (type A) match the value of 7 ± 3 fs found in non-spin-resolved 2PPE [30]. The lower-work-function (type B) samples show larger lifetimes. At first glance this is surprising, since scattering at defects is known to lead to a decrease of the image-potential-state lifetimes [40]. The increase of lifetime indicates a loss of

decay channels.

In the relaxation process the unoccupied final states are populated by the image-potential-state electron and by the generation of a secondary electron-hole pair conserving energy and momentum. The Shockley surface state serves as prominent final state in electron-electron scattering due to the preferred large energy and small momentum transfer in inelastic electron-electron scattering [41]. Therefore we attribute the longer lifetimes to a partial quenching of the surface state near E_F .

A surface-quality-dependent change in the $n = 1$ image-potential-state lifetime has been observed before by Link *et al.* [30]. They reported an increase in lifetime upon hydrogen adsorption accompanied by a quenching of the Shockley surface state. Fischer *et al.* observed the same effect in a decrease in linewidth of the $n = 1$ image-potential state [5]. These observations corroborate that the Shockley surface state serves as a major decay channel for the electrons excited into the image-potential state. Note that in our measurements the increase of the lifetime from type A to type B samples is about 40 % of the type B lifetime, which resembles the contribution of the Shockley state to the $n = 1$ image-potential-state decay-rate calculated for the Cu(111) surface by Chulkov *et al.* [41].

There is a small spin asymmetry in the lifetimes that is corroborated by the temporal evolution of the spin polarization shown in the mid part of Fig. 6. The spin polarization is negative meaning that the initial state population excited to the image-potential state has minority spin character. With increasing pump-probe delay the polarization decreases by 20 % reflecting that the minority spin population is decaying faster than that of the majority spin electrons. The $n = 1$ image-potential-state lifetime-asymmetry $\tau^\uparrow/\tau^\downarrow = 1.27$ on Ni(111) is lower than on Fe (1.45) and Co (1.6) thin films on Cu(001) [24]. This supports the trend that has been predicted by Grechnev *et al.* for bulk states with slightly lower energies above the Fermi level [42]. A recent calculation of hot electron lifetimes by Kaltenborn and Schneider, which includes spin-orbit coupling and thus spin-mixing in the band structure, finds a different order for $\tau^\uparrow/\tau^\downarrow$ (Fe < Co < Ni) [43].

With increasing lifetime from sample type A to sample type B the lifetime asymmetry decreases. This can also be attributed to a partial quenching of the Shockley surface state, which is completely unoccupied in the minority but partly occupied in the majority spin channel. Therefore it constitutes an additional spin-dependent decay channel, which is of importance due to the large spatial overlap of image-potential and Shockley surface state.

All literature values stem from measurements on single crystal surfaces [5, 30]. As mentioned before in Sec. 1 and 2.1, in thin nickel films deposited on W(110) the formation of QWS is possible as has been observed in Ref. [21]. These interface states could provide additional decay channels for the image-potential-state electrons. Despite the fact that the number of quantum-well states around the Fermi level is found to increase with the number of Ni layers, we have not observed any dependence of the image-potential-state lifetimes on the film thickness in the range from 7 to 14 ML. This

Table 2. Comparison of work function, lifetimes and spin asymmetries of the $n = 1$ image-potential state for samples A and B.

Sample type	Work function (eV)	$\tau_{\uparrow}(fs)$	$\tau_{\downarrow}(fs)$	$\tau_{\uparrow/\downarrow}$
A	5.27 ± 0.03	11.3 ± 0.3	8.9 ± 0.5	1.27 ± 0.06
B	5.11 ± 0.03	19.3 ± 2.6	17.6 ± 2.5	1.10 ± 0.20

corroborates our findings that the electronic structure of our films is characteristic for the Ni(111) surface and does not exhibit QWS.

4.4. Linewidths

The linewidths measured in 2PPE provide additional information about quasi-elastic scattering processes [44]. In 2PPE the laser field induces a superposition of electronic states. Scattering processes with an energy transfer lower than the experimental resolution (quasi-elastic) do not contribute to the electronic relaxation process but lead to a dephasing of this superposition, *i.e.*, the polarization. This results in a broadening of the spectral linewidth. A spin asymmetry in dephasing rates can be caused by electron-magnon scattering as it has been shown for 3 ML Fe/Cu(001) [45]. Here spin-wave emission leads to an additional linewidth broadening of the $n = 1$ minority image-potential state.

The lower part of Fig. 6 shows the temporal evolution of the Lorentzian linewidth of the $n = 1$ image-potential state. The pure dephasing rate gives a constant offset to the linewidth. It can be observed at large positive pump-probe delays. For negative pump-probe delays the linewidth increases due to the decreasing overlap of the $h\nu$ probe and $3h\nu$ pump pulse as seen in Fig. 6. Besides the laser pulse-widths an additional broadening may occur caused by a contribution of a particular initial state. We interpret the different linewidth for majority and minority $n = 1$ image-potential states at negative delay as an effect induced by different initial states for the two spin directions (see Fig. 2).

In the region of zero pump-probe delay where initial and image-potential states overlap in time, the linewidth of the 2PPE peak is decreasing until it reaches a constant value of 25 meV for large positive delays which is twice the pure dephasing rate. Unlike for the image-potential states on Fe/Cu(001) we cannot find a significant spin asymmetry in the dephasing rate for Ni/W(110). This corroborates the low probability of magnon emission predicted for Ni [46] leading to the low significance of spin-flip contributions to electronic decay [3]. The dephasing rate $\hbar\Gamma^* \approx 12$ meV corresponds to the dephasing rate of the majority spin component of the $n = 1$ image-potential state on Fe/Cu(001) [45] which is likewise unaffected by magnon emission.

5. Conclusion

In summary our data collected with the superior surface sensitivity of 2PPE support the predictions from recent band structure calculations [7, 9]. The majority spin component of the Shockley surface state is occupied with a binding energy of ≈ 150 meV at a sample temperature of 90 K. Its minority component is unoccupied and there is no sign of minority spin character around E_F . However, we clearly find a surface state with minority spin character at a binding energy $E_F - 230$ meV. Since this state is derived from the d bands that are exchange split by about 160 – 250 meV, [47, 48] we expect its majority counterpart at about $E_F - 500$ meV. We give evidence for two majority surface states at 289 meV and at ≈ 500 meV, as predicted in Refs. [7, 9, 20].

For the image-potential states we determine binding energies lower than those measured in non-spin-resolved 2PPE but higher than those determined by inverse photoemission on Ni(111) single crystals. The exchange splitting of 14 ± 3 meV for the $n = 1$ image-potential states is the smallest of the known values for the ferromagnetic surfaces of the 3d-transition metals. Nevertheless, it agrees with the value of 16 meV expected from the bulk penetration of the image-potential state alone.

The small exchange splitting of valence and image-potential states is reflected in the low spin asymmetries of the inelastic as well as quasi-elastic scattering rates. The asymmetric spin-dependent DOS at the Fermi level effects the decay of the image-potential-state population much less than it has been predicted for hot bulk electrons by *ab initio* calculations [42, 49]. We find the lifetime of majority spin electrons in the $n = 1$ image-potential state to be only a factor of $\tau_{\uparrow/\downarrow} = 1.27 \pm 0.06$ larger than that of the minority spin electrons. This ratio is even smaller for samples with lower work function. We attribute the latter to a partial quenching of the Shockley surface state, which constitutes an effective spin-dependent decay channel. Compared to the measured lifetime asymmetry theory predicts significantly larger values of $\tau_{\uparrow/\downarrow} \simeq 5$ [46, 49, 42]. Including spin mixing, recent calculations support lower lifetime asymmetries but still overestimate $\tau_{\uparrow/\downarrow} \simeq 2$ for nickel [43]. The dephasing rate of the $n = 1$ image-potential state shows no spin dependence corroborating the minor role of magnon emission for electron scattering in nickel predicted in Refs. [46, 49].

In line with the experimentally observed low lifetime asymmetry of hot bulk electrons in nickel [50, 51] the electron dynamics at the Ni(111) surface show a small spin-dependence. With no signature of magnon emission, low-energy spin-flip scattering seems to play a minor role. Furthermore, we observe a surface-state-enhanced spin-asymmetry of the lifetime. We therefore propose that also spin-dependent transmission barriers play a role for the highly spin-polarized electron emission in nickel hybrid-systems [2].

Acknowledgments

We thank A.B. Schmidt and M. Donath for valuable discussions and acknowledge the *Deutsche Forschungsgemeinschaft* for financial support.

References

- [1] Alvarado S F and Renaud P, *Phys. Rev. Lett.* **68**, 1387 (1992).
- [2] Dedkov Y S, Fonin M, and Laubschat C, *Applied Physics Letters* **92**, 052506 (2008).
- [3] Zhukov V P, Chulkov E V, and Echenique P M, *Phys. Rev. Lett.* **93**, 096401 (2004).
- [4] Echenique P M and Pendry J B, *J. Phys. C. Sol. State Phys.* **11**, 2065 (1978).
- [5] Fischer N, Schuppler S, Fauster T, and Steinmann W, *Phys. Rev. B* **42**, 9717 (1990).
- [6] Dzemiantsova L V *et al.*, *Phys. Rev. B* **84**, 205431 (2011).
- [7] Lobo-Checa J, Okuda T, Hengsberger M, Patthey L, Greber T, Blaha P, and Osterwalder J, *Phys. Rev. B* **77**, 075415 (2008).
- [8] Borstel G, Thörner G, Donath M, Dose V, and Goldmann A, *Solid State Communications* **55**, 469 (1985).
- [9] Ohwaki T, Wortmann D, Ishida H, Blügel S, and Terakura K, *Phys. Rev. B* **73**, 235424 (2006).
- [10] Braun J and Donath M, *EPL (Europhysics Letters)* **59**, 592 (2002).
- [11] Kutzner J, Paucksch R, Jabs C, Zacharias H, and Braun J, *Phys. Rev. B* **56**, 16003 (1997).
- [12] Higashiguchi M, Shimada K, Arita M, Miura Y, Tobita N, Cui X, Aiura Y, Namatame H, and Taniguchi M, *Surface Science* **601**, 4005 (2007).
- [13] Nishimura Y, Kakeya M, Higashiguchi M, Kimura A, Taniguchi M, Narita H, Cui Y, Nakatake M, Shimada K, and Namatame H, *Phys. Rev. B* **79**, 245402 (2009).
- [14] Kämper K-P, Schmitt W, Güntherodt G, and Kühlenbeck H, *Phys. Rev. B* **38**, 9451 (1988).
- [15] Rhie H-S, Dürr H A, and Eberhardt W, *Phys. Rev. Lett.* **90**, 247201 (2003).
- [16] Donath M, Passek F, and Dose V, *Phys. Rev. Lett.* **70**, 2802 (1993).
- [17] Braun K-F and Rieder K-H, *Phys. Rev. B* **77**, 245429 (2008).
- [18] Krönlein A, Kemmer J, Hsu P-J, and Bode M, *Phys. Rev. B* **89**, 155413 (2014).
- [19] Himpfel F J and Eastman D E, *Phys. Rev. Lett.* **41**, 507 (1978).
- [20] Okuda T *et al.*, *Phys. Rev. B* **80**, 180404 (2009).
- [21] Nuber A, Ph.D. thesis, University of Würzburg, 2011.
- [22] Pickel M, Schmidt A B, Giesen F, Braun J, Minár J, Ebert H, Donath M, and Weinelt M, *Phys. Rev. Lett.* **101**, 066402 (2008).
- [23] Schmidt A B, Pickel M, Wiemhofer M, Donath M, and Weinelt M, *Phys. Rev. Lett.* **95**, 107402 (2005).
- [24] Weinelt M, Schmidt A, Pickel M, and Donath M, *Progress in Surface Science* **82**, 388 (2007).
- [25] Zakeri K, Peixoto T, Zhang Y, Prokop J, and Kirschner J, *Surf. Sci.* **604**, L1 (2010).
- [26] Eickhoff C, Teichmann M, and Weinelt M, *Phys. Rev. Lett.* **107**, 176804 (2011).
- [27] Hermanson J, *Solid State Communications* **22**, 9 (1977).
- [28] Auwärter W, Ph.D. thesis, University of Zürich, 2003.
- [29] Passek F and Donath M, *Phys. Rev. Lett.* **69**, 1101 (1992).
- [30] Link S, Sievers J, Dürr H, and Eberhardt W, *Journal of Electron Spectroscopy and Related Phenomena* **114-116**, 351 (2001).
- [31] Smoluchowski R, *Phys. Rev.* **60**, 661 (1941).
- [32] Leung T C, Kao C L, Su W S, Feng Y J, and Chan C T, *Phys. Rev. B* **68**, 195408 (2003).
- [33] Wortelen H, Diplomarbeit, Westfälische Wilhelms-Universität Münster, 2011.
- [34] Schuppler S, Fischer N, Steinmann W, Schneider R, and Bertel E, *Phys. Rev. B* **42**, 9403 (1990).
- [35] Steinmann W, *Applied Physics A* **49**, 365 (1989).

- [36] Fauster T and Steinmann W, in *Photonic Probes of Surfaces*, edited by Halevi P (North-Holland, Amsterdam, 1995), Vol 2, p. 347.
- [37] Braun J, Borstel G, and Nolting W, *Phys. Rev. B* **46**, 3510 (1992).
- [38] Wolf M, *Surface Science* **377-379**, 343 (1997), european Conference on Surface Science.
- [39] Weinelt M, *J. Phys.: Condens. Matter* **14**, R1099 (2002)
- [40] Boger K, Weinelt M, and Fauster T, *Phys. Rev. Lett.* **92**, 126803 (2004).
- [41] Chulkov E V, Sarria I, Silkin V M, Pitarke J M, and Echenique P M, *Phys. Rev. Lett.* **80**, 4947 (1998).
- [42] Grechnev A, Di Marco I, Katsnelson M I, Lichtenstein A I, Wills J, and Eriksson O, *Phys. Rev. B* **76**, 035107 (2007).
- [43] Kaltenborn S and Schneider H C, arXiv:1403.4728 (2014).
- [44] Boger K, Roth M, Weinelt M, Fauster T, and Reinhard P, *Phys. Rev. B* **65**, 075104 (2002).
- [45] Schmidt A B, Pickel M, Donath M, Buczek P, Ernst A, Zhukov V P, Echenique P M, Sandratskii L M, Chulkov E V, and Weinelt M, *Phys. Rev. Lett.* **105**, 197401 (2010).
- [46] Hong J and Mills D L, *Phys. Rev. B* **62**, 5589 (2000).
- [47] Kämper K-P, Schmitt W, and Güntherodt G, *Phys. Rev. B* **42**, 10696 (1990).
- [48] Greber T, Kreuz T J, and Osterwalder J, *Phys. Rev. Lett.* **79**, 4465 (1997).
- [49] Zhukov V P, Chulkov E V, and Echenique P M, *Phys. Rev. B* **73**, 125105 (2006).
- [50] Aeschlimann M, Bauer M, Pawlik S, Weber W, Burgermeister R, Oberli D, and Siegmann H C, *Phys. Rev. Lett.* **79**, 5158 (1997).
- [51] Goris A, Ph.D. thesis, Freie Universität Berlin, 2010.